

Double Resonance NMR and Molecular Simulations of Hydrofluorocarbon Binding on Faujasite Zeolites NaX and NaY: the Importance of Hydrogen Bonding in Controlling Adsorption Geometries

Kwang Hun Lim,^{†,||} Fabien Jousse,^{‡,⊥} Scott M. Auerbach,^{‡,§} and Clare P. Grey^{*,†}

Department of Chemistry, SUNY Stony Brook, Stony Brook, New York 11794-3400, Department of Chemistry, University of Massachusetts, Amherst, Massachusetts 01003, and Department of Chemical Engineering, University of Massachusetts, Amherst, Massachusetts 01003.

Received: December 31, 2000; In Final Form: May 8, 2001

Double resonance NMR experiments have been used to study the binding of the asymmetric hydrofluorocarbons (HFCs) CF₃CFH₂ (HFC-134a), CF₃CF₂H (HFC-125) and CF₂HCFH₂ (HFC-143) on zeolites NaX and NaY. By exploiting the very large differences in ¹⁹F chemical shifts for the –CF_{3–x}H_x end groups of each molecule, individual ¹⁹F → ²³Na cross-polarization (CP) build-up curves involving polarization transfer from different parts of the molecule have been obtained. CP efficiencies in the order CF₃ ≪ CF₂H < CFH₂ were found, indicating that the hydrogen-containing groups are bound more strongly to the zeolite framework. This effect is most pronounced for the lowest-sodium content zeolite studied (NaY: Si/Al = 7.6), and increases with HFC loading. Both the ¹H NMR resonances and ¹H → ²⁷Al and ¹H → ¹⁷O CP MAS NMR experiments are consistent with H-bonding interactions with the zeolite framework. Molecular dynamics and docking calculations for HFC-134 and 134a on model NaY and NaX zeolites revealed the importance of *both* H-bonding and Na–F interactions in determining the low-energy sorption sites. Stable binding sites for HFC-134a in NaY were found by docking to involve only CFH₂–Na(SII) contacts, in qualitative agreement with the CP results. The simulations indicate that Na-binding to the groups with more H atoms is favored by the possibility of achieving shorter Na–F distances *and* maximizing the number of H-bonds with the framework. The higher sodium content zeolite containing both SII and SIII cations gives minimum energy binding sites involving multiple Na–F and H-bonding contacts. For HFC-134 (gauche conformer), the global energy minimum actually involves several H-bonds but no short Na–F contacts.

1. Introduction

Hydrofluorocarbons (HFCs) are now widely used as alternatives to chlorofluorocarbons (CFCs) in a wide range of applications, which include refrigeration, blowing agents and aerosols. However, the syntheses of the HFCs are more complex than the syntheses of CFCs and involve many more steps.¹ Unwanted HFC, hydrochlorofluorocarbon (HCFC) and CFC isomers are often produced during the reactions: for example, CF₂HCF₂H (HFC-134) is a common byproduct in the synthesis of CF₃CFH₂ (HFC-134a), the replacement for the refrigerant CFC-12 (CF₂Cl₂).¹ Basic molecular sieves have been proposed as a method for separating some of these isomer mixtures² and can also be used as drying agents, following scrubbing to remove HF. HFC-134 molecules are known to bind more tightly to the zeolites than HFC-134a molecules,³ the separation factor for the HFC-134/-134a mixture anti-correlating with the Sanderson electronegativity of the monovalent cation-exchanged forms of zeolites Y, increasing from Li, Na, K to CsY.²

We have been applying a variety of NMR and X-ray powder diffraction methods to determine the importance of different

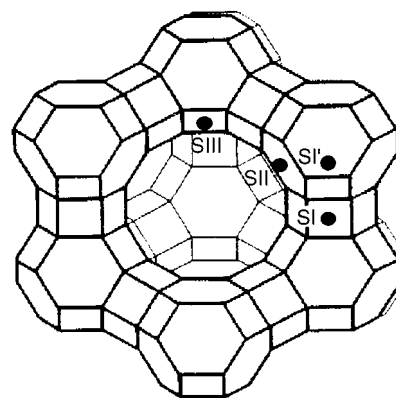


Figure 1. Faujasite structure (adopted by zeolites NaY and NaX), showing typical (idealized) cation positions.

interactions in controlling the sorption properties of these gases on faujasite zeolites, and to understand in more detail the separation behavior and HFC reactivity.^{4,5} Our previous combined X-ray diffraction and solid-state NMR study on the binding of HFC-134 on zeolite NaY demonstrated that Na–F interactions play an important role in these systems, and are strong enough to cause migration of cations from the SI' positions in the sodalite cages (shown in Figure 1) into the supercage where they can bind to both ends of the HFC molecule.⁵ More recently, more sophisticated NMR techniques were applied to this problem and cation migrations in NaY

[†] Department of Chemistry, SUNY Stony Brook.

[‡] Department of Chemistry, University of Massachusetts.

[§] Department of Chemical Engineering, University of Massachusetts.

^{||} Present address: Department of Chemistry, University of California, Berkeley, CA 94720.

[⊥] Present address: Unilever Research, Olivier van Noort Laan 120, 3133 AT Vlaarding, the Netherlands.

induced by a wide variety of HFCs, including (HFC-134, HFC-134a, CF₃CF₂H (HFC-125), and CF₂HCFH₂ (HFC-143)) were observed.⁶

In other experiments, we have exploited the cross-polarization (CP) double resonance method to investigate the binding of asymmetric HFCs (HFC-134a, -125, and -143) on zeolites NaX and NaY. We reported a short communication describing the results for sorption on NaY, which indicated that the larger the number of hydrogen atoms in the end group of the molecule, the stronger the interaction of this end group with the framework.⁷ These results present two surprises based on naïve expectations. First, HFC-134 binds more favorably to faujasite-type zeolites than does HFC-134a, despite the chemical symmetry of HFC-134 and the permanent dipole of HFC-134a (ca. 1.8 D). Even more surprising is the fact that, for HFC-134a, the -CFH₂ group enjoys stronger attractions to Na(II) in the supercage than does the -CF₃ group, despite the greater number of electronegative atoms in -CF₃. If correct, these results indicate that simple intuition, based either on overall molecular dipole moments or on counting the number of Na-F contacts, can fail to describe the details of HFC adsorption in zeolites. To test the validity of these surprising findings, we have examined these systems in more detail with two independent and complementary probes of local structure: solid-state NMR and computer simulations.

The present studies were performed to determine: (i) the preferential binding of the different HFC end groups, and (ii) the relative importance of the hydrogen bonding^{8,9} vs Na-F interactions, both as a function of the HFC and the sodium content of the zeolite. To address these issues, the results from various NMR probes of the dynamics and binding are presented first. Calculations are then reported for two model zeolites, one containing a low sodium content (NaY, Si/Al = 2) and the other a higher content (NaX, Si/Al = 1); experimental and simulation results are then compared. By structuring the paper in this way, we hope to develop a qualitative picture for the nature of HFC binding in zeolites, especially for asymmetric HFCs, which will then be corroborated by comparing the experimental and simulation results. In general, we find from both experiment and simulation that the -CFH₂ group in HFC-134a is indeed much closer to supercage cations, and that hydrogen bonds play a very important role in determining the details of HFC adsorption in zeolites.

2. Methods

Experimental. (a) *Sample Preparation.* Zeolites NaX and NaY_{2.6} used in this study were commercial products (Aldrich and Strem chemicals, respectively). Zeolite NaY_{7.6} and the different gases were provided by Dr. D. R. Corbin at DuPont CR&D. Prior to the NMR experiments, each zeolite sample was dehydrated on a vacuum line by slowly ramping the temperature to 400 °C over a period of 48 h. HFC adsorptions were also performed on the vacuum line by introducing controlled amounts of the gas in a closed line and exposing the gas to the dehydrated zeolite samples at room temperature. Samples are labeled xHFC/zeolite, where *x* indicates the number of HFC molecules per supercage (sc). The amount of gas adsorbed was determined by observing the pressure drop with an absolute pressure Phillips-Granville gauge. Fully loaded samples were prepared by exposing the samples to the gas until no further drop in pressure was observed. All samples were then packed in ZrO₂ rotors for NMR experiments in a glovebox under dry N₂. ICP elemental analysis of the original hydrated sample of NaY_{2.6} gave a composition (by weight percentage) of Na:6.94(4); Si:

22.2(2); Al:8.26(6), leading to a composition of the unit cell of Na_{52.8}Si_{138.4}Al_{53.6}O₃₈₄. Si/Al ratios for NaX (1.25) and NaY_{7.6} (7.6) were determined from their ²⁹Si MAS NMR spectra. For the ¹⁷O NMR experiments, ¹⁷O-enriched zeolite NaY_{2.6} was prepared by heating dehydrated NaY_{2.6} for 12 h at 600 °C, under 2 atm pressure of 50% ¹⁷O₂ enriched gas (from Isotec).

(b) *NMR.* All of the MAS NMR spectra were acquired with a double-tuned 5 mm Chemagnetics probe, on a CMX-360 spectrometer with resonance frequencies for ¹⁹F and ²³Na of 338.7 and 95.2 MHz, respectively. ¹H static NMR spectra were acquired with a 4 mm Chemagnetics probe, on a CMX-200 spectrometer at 200.15 MHz. The chemical shifts reported were referenced to external standards: CFCI₃ for ¹⁹F, solid NaCl for ²³Na, 1 M Al₂(SO₄)₃ for ²⁷Al, distilled water for ¹⁷O and TMS for ¹H, all at 0.0 ppm. Samples were spun at speeds of 8 to 10 kHz. Lead(II) nitrate (Pb(NO₃)₂)¹⁰ was used to calibrate the Chemagnetics VT equipment used for this study and the temperature under static conditions was assumed to be identical to that under slow MAS conditions (2.5 kHz). Rf field strengths of ~10–20 kHz and ~20–40 kHz were used for ²³Na and ¹⁹F, respectively, for the ¹⁹F → ²³Na CP MAS NMR experiments, to match the Hartmann–Hahn condition for quadrupolar nuclei with nonzero quadrupole coupling constants.^{11,12} These CP conditions correspond to the sudden-passage regime where adiabatic passages between the eigenstates of quadrupolar nuclei spin systems do not occur. For CP MAS experiments involving other quadrupolar nuclei (²⁷Al and ¹⁷O), low rf field strengths for quadrupolar nuclei and fast spinning speeds (i.e., the sudden-passage condition) were also used to help ensure effective spin-locking for the quadrupolar nuclei.^{11–14} All quoted rf field strengths correspond to those measured with a liquid sample.

The CP approach exploits the fact that the two resonances for the different CF_{3–n}H_n groups are well separated in the ¹⁹F NMR spectra of the asymmetric HFCs: for example, the chemical shifts for the CF₃ and CFH₂ groups of HFC-134a are -81 and -246 ppm, respectively. The CP efficiency is very sensitive to the offset-frequency of the ¹⁹F rf field, the polarization transfer rate decreasing by an amount:

$$\nu_1^2/(\nu_1^2 + \delta_{\text{off}}^2) \quad (1)$$

as the offset frequency (δ_{off}) of the applied rf field (ν_1) is increased. Thus, if the ¹⁹F frequency difference between different end groups of the HFCs (58, 18, and 40 kHz for HFC-134a, -125 and -143, respectively at a field strength of 8.45 T) is large compared to the rf field strength (typically, 20–40 kHz), the CP dynamics of the two groups may be investigated separately.

Numerical simulations were performed in the GAMMA¹⁵ environment. A three Euler angle set (3722 orientations), chosen with the ZCW algorithm,¹⁶ was used for the simulation of the powder.

Simulations. (a) *Models and Forcefield.* We should first note that our aim in performing simulations on this system is not to reproduce the experimental results quantitatively, but to look for possible explanations of the experimental findings. We, therefore, used simplified models for the zeolite structures as well as simplified potentials and simulation procedures. In particular, the framework was kept rigid and the cations were fixed in their original positions during all the simulations.

To capture some of the structural variety in faujasite zeolites, we used two models with different cation distributions. Model I (NaY) corresponds to a faujasite structure with Si/Al = 2, with complete filling of cation sites I' and II, while model II corresponds to bare NaX (Si/Al = 1), also with complete filling

of sites I' and II, but with the remaining cations occupying sites III above a 4-T ring in a 12-T window. Models I and II were previously used by Auerbach and co-workers to model the adsorption of benzene in NaY and NaX, respectively.¹⁷

X-ray crystallographic data from Fitch et al.¹⁸ were used to build the faujasite framework of model I and to locate the cations. For model II, we used the structure of Hseu, with cations occupying SIII, in addition to the SI, SI' and SII sites. We also considered an alternative model for NaX with Si/Al = 1.2, from Vitale et al.,¹⁹ where cations occupy sites III' above an O–T–O site in a 12-T window. However, this model led to unrealistically large interaction energies with HFC-134 (up to 191 kJ/mol), as well as with benzene.²⁰ These high energies probably arise because of the assumed cation distribution in sites III'; if these were allowed to relax, repulsive cation–cation interactions would likely force these III' cations into locations that would not bind so strongly to the HFCs. For this reason, in the following, we will only give the results obtained for models I and II.

We used the CVFF force field from MSI for guest internal and guest-zeolite interactions in all simulations, within the average T-site approximation, in which all Si or Al atoms are considered equivalent and assigned an average charge that depends on the Si/Al ratio. The use of this model simplifies the interpretation of the results, since we do not consider the possible heterogeneity of the Al distribution. Similar average T-sites models have been shown to give quantitative agreement with calorimetric experiments for the adsorption of chloroform in faujasite zeolites.²¹ The CVFF force field has been previously used by George et al. to study the adsorption of HFCs and CFCs in zeolites of different topologies.²² Parameters from the CVFF force field were implemented inside the Dizzy computational chemistry code.²³ The energy is computed as the sum of guest internal (U_g) and guest-zeolite (U_{gz}) interactions

$$U = U_g + U_{gz}$$

$$U_g = \sum_{\text{bonds}} \frac{1}{2} K_b (r - r_0)^2 + \sum_{\text{angles}} \frac{1}{2} K_\theta (\theta - \theta_0)^2 + \sum_{\text{torsions}} K_\phi (1 + \alpha \cos \beta\phi) \quad (2)$$

$$U_{gz} = \sum_{i,j>i} \left[\frac{A_{ij}}{r_{ij}^{12}} - \frac{B_{ij}}{r_{ij}^6} + \frac{q_i q_j}{r_{ij}} \right]$$

Lennard–Jones parameters A_{ij} and B_{ij} are determined from “atomic” parameters A_1 and B_1 using the following combination rule:

$$A_{ij} = \sqrt{A_i A_j}, B_{ij} = \sqrt{B_i B_j}. \quad (3)$$

Parameters for guest internal and guest-zeolite interactions are given in Tables 1 and 2, respectively.

(b) *Sampling Methods.* The adsorption and dynamics of HFC-134 and HFC-134a in faujasites were investigated by using two standard techniques: docking and molecular dynamics. In both cases, we only considered one molecule in a simulation cell consisting of 8 superpages of the material, under periodic boundary conditions.

We used the docking procedure described by Auerbach et al. in ref 17: a series of minimum energy conformations for a single guest molecule within the zeolite were first generated by giving the adsorbate a random translational kick. This was

TABLE 1: Interaction Parameters for Guest Internal Interactions, from the CVFF Forcefield of MSI

quadratic bond: $E = 1/2K_b(r - r_0)^2$			
species	K_b (eV/Å ²)	r_0 (Å)	
C–C	27.988	1.526	
C–H	29.540	1.105	
C–F	43.016	1.363	
quadratic angle: $E = 1/2K_\theta(\theta - \theta_0)^2$			
species	K_θ (eV/rad ²)	θ (degrees)	
F–C–C	8.586	107.8	
F–C–H	5.378	107.1	
H–C–H	3.426	106.4	
H–C–C	3.816	110.0	
F–C–F	4.042	109.5	
torsion angle: $E = K_\phi[1 + \alpha \cos \beta\phi]$			
species	K_ϕ (eV)	α	β
–C–C–	0.0617	1.0	3.0

TABLE 2: Interaction Parameters for Guest-Zeolite Interactions, from the Forcefield CVFF of MSI

species	A (kcal/mol Å ¹²)	B (kcal/mol Å ⁶)	q (e)
C ^a	1790340.724	528.4819	+0.45
C ^b	1790340.724	528.4819	+0.075
C ^c	1790340.724	528.4819	+0.825
H	7108.466	32.8708	+0.1
F	201106.0	235.2	–0.275
T ^d	3149175.0	710.0	+1.0367
T ^e	3149175.0	710.0	+0.87
O	272894.7846	498.8788	–0.685
Na	14000.0	300.0	+1.0

^a Carbon atom in HFC-134. ^b Carbon atom in a CFH₂ group. ^c Carbon atom in a CF₃ group; ^d T atom in model I (Si/Al = 2); ^e T atom in model II (Si/Al = 1).

followed by 1000 steps of high-temperature molecular dynamics (MD), and the resulting structure was then quenched. It was necessary to run the MD at a temperature of 10 000 K to sample the F–C–C–F torsion angle. One hundred structures were generated for both HFC-134 and HFC-134a in each model. Because this represents a high-symmetry system, this number of structures should guarantee that most energy minima are located.

Molecular dynamics runs were started from the absolute minimum energy position located by the docking procedure. A 100 ps equilibration run was performed in the NVT ensemble at 300 K, followed by a 0.4 ns production run in the NVE ensemble, with a time step of 1 fs. The NVT runs were constrained using the Berendsen thermostat with a long coupling time of 100 ps. Conformations were stored every 20 fs for subsequent analysis. From the production run we computed pair distribution functions (PDFs) between atom types A and B

$$\rho_{AB}(r) = \frac{1}{r^2} \langle \delta(r_{AB} - r) \rangle \quad (4)$$

normalized so that $\int \rho_{AB}(r) r^2 dr = 1$.

3. Results

NMR. (a) ¹⁹F → ²³Na CP MAS. Figure 2 shows the ²³Na MAS (a), and the ¹⁹F → ²³Na CP MAS spectra of fully loaded HFC-134a/NaY_{2.6} at –120 °C, for ¹⁹F irradiation frequencies placed on the CF₂H group (b), and the CF₃ group resonances (c). The sharp ²³Na resonance at ~–10 ppm, from the site I cations in the double six ring, is not observed in the CP MAS

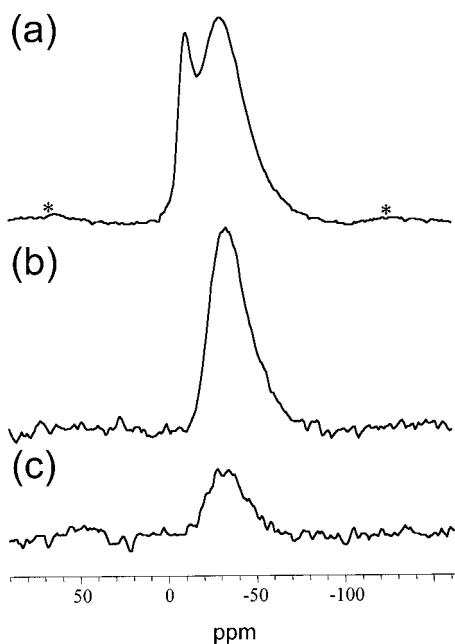


Figure 2. (a) ^{23}Na MAS NMR spectra of fully loaded HFC-134a/ $\text{NaY}_{2.6}$ at -120°C . Spinning speeds of 10 kHz were used. (b) and (c): The $^{19}\text{F} \rightarrow ^{23}\text{Na}$ CP MAS spectra of fully loaded HFC-134a/ $\text{NaY}_{2.6}$ at -120°C . The ^{19}F frequency was placed on resonance for the CFH_2 resonance and CF_3 resonance in (b) and (c), respectively. Spinning speeds of 9.5 kHz, a 400 μs CP contact time (τ), an ^{19}F rf field strength, $\nu_{1\text{F}}$, of 40 kHz and an ^{23}Na rf field strength, $\nu_{1\text{Na}}$, of 20 kHz were used and 1640 acquisitions were recorded for each spectrum. The "*" denote spinning sidebands.

spectra, while the broad resonances at ~ -35 and -50 ppm are both present. We have obtained similar results for HFC-134 and 134a sorption in our earlier study, and based on a combination of ^{23}Na MAS, $^{19}\text{F} \rightarrow ^{23}\text{Na}$ CP MAS and MQMAS NMR, have assigned these two broad resonances to site II and III (or III') cations, respectively, the latter resulting from the cation migration from the sodalite cage to the supercage on adsorption of the HFC molecules.⁶ The CP intensity is much higher for CP from the CF_2H group, in comparison to CP from the CF_3 group, which contains more fluorine spins, indicating that ^{19}F to ^{23}Na magnetization transfer from the CFH_2 group is more efficient than from the CF_3 group. To investigate this behavior fully, CP experiments were performed as a function of fluorine irradiation offset and loading level for HFC-134a, -125, -143 (Figure 3a–c) adsorbed on $\text{NaY}_{2.6}$. A dramatic decrease in ^{23}Na CP intensity for 4HFC-134a/ $\text{NaY}_{2.6}$ is observed, as the fluorine irradiation offset δ_{off} is changed from on-resonance for the CFH_2 group (-58 kHz) to on-resonance for the CF_3 group (0 kHz). The CP intensity for 4HFC-125/ $\text{NaY}_{2.6}$ drops steadily as the offset frequency is increased, reaching zero when $\delta_{\text{off}} = 50$ kHz (measured relative to the CF_3 group) (Figure 3b). The intensity for irradiation at the CFH_2 group frequency is a little higher than that for irradiation of the CF_3 group, even though the latter has more fluorine atoms. The frequency difference between the two end groups of HFC-125 (18 kHz) is smaller than the ^{19}F rf field strength (34 kHz), hence there will be a significant overlap of the two CP profiles for the two end groups. Experiments were, therefore, repeated with a lower ^{19}F rf field strength (20 kHz). The CP intensity for irradiation at the CF_3 group frequency now drops to 70% of the CP intensity for irradiation of the CFH_2 group. The same experiment was performed for 4HFC-143/ $\text{NaY}_{2.6}$ at three temperatures (-120 , -110 , and -100°C). The CP intensity for on-resonance irradiation of the CFH_2 group increased as the temperature was

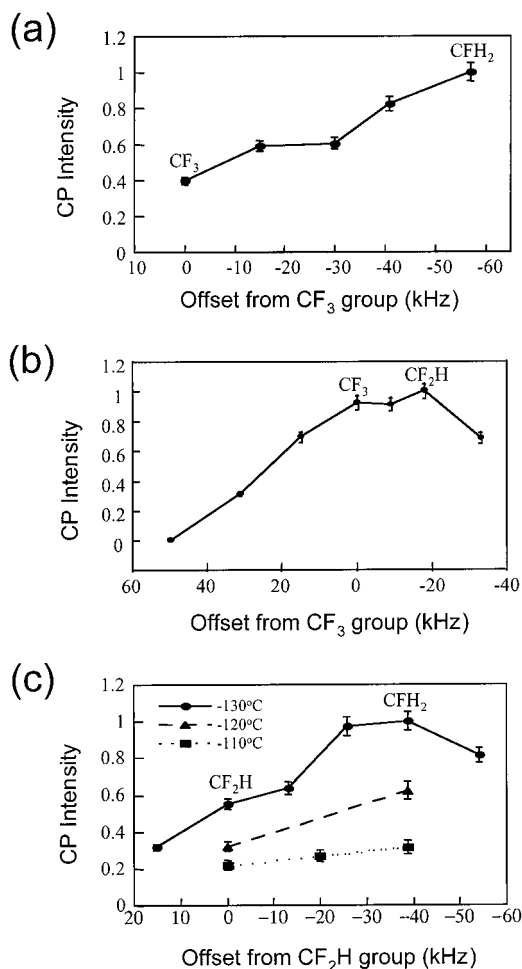


Figure 3. $^{19}\text{F} \rightarrow ^{23}\text{Na}$ CP intensity as a function of fluorine irradiation offset of (a) 4HFC-134a/ $\text{NaY}_{2.6}$ at -120°C . (Spinning speed = 9 kHz; $\tau = 333 \mu\text{s}$; $\nu_{1\text{F}} = 40$ kHz; $\nu_{1\text{Na}} = 20$ kHz). (b) 4HFC-125/ $\text{NaY}_{2.6}$ at -120°C . (Spinning speed = 8.5 kHz; $\tau = 350 \mu\text{s}$; $\nu_{1\text{F}} = 34$ kHz; $\nu_{1\text{Na}} = 17$ kHz). (c) 4HFC-143/ $\text{NaY}_{2.6}$ at -110 , -120 and -130°C . (Spinning speed = 8 kHz; $\tau = 250 \mu\text{s}$; $\nu_{1\text{F}} = 20$ kHz; $\nu_{1\text{Na}} = 10$ kHz).

lowered, and was higher than that for the CF_2H group at all temperatures (Figure 2c).

The $^{19}\text{F} \rightarrow ^{23}\text{Na}$ CP intensity was measured as a function of the contact time for the three samples, the CP intensity from the more hydrogenated groups growing faster than the CP intensity from the other groups (Figure 4). A simulation has been performed to fit the CP curves with following equations:^{14,24,25}

$$\beta_s(t) = \beta_I^0 \frac{1}{a_+ - a_-} [e^{-a_-t/T_{1\text{S}}} - e^{-a_+t/T_{1\text{S}}}] \quad (5)$$

where

$$a_{\pm} = c \left\{ 1 \pm \left[1 - \frac{T_{1\text{S}}^I/T_{1\rho}^I (1 + T_{1\text{S}}^S/T_{1\rho}^S) + \epsilon T_{1\text{S}}^S/T_{1\rho}^S}{c^2} \right]^{1/2} \right\} \quad (6)$$

$$c = \frac{1}{2} \left(1 + \epsilon + \frac{T_{1\text{S}}}{T_{1\rho}^I} + \frac{T_{1\text{S}}}{T_{1\rho}^S} \right) \quad (7)$$

$$\epsilon = \frac{N_{\text{S}}S(S+1)\gamma_{\text{S}}^2 B_{1\text{S}}^2}{N_{\text{I}}I(I+1)\gamma_{\text{I}}^2 B_{1\text{I}}^2} \quad (8)$$

where β and $1/T_{1\text{S}}$ are the inverse spin temperature and the

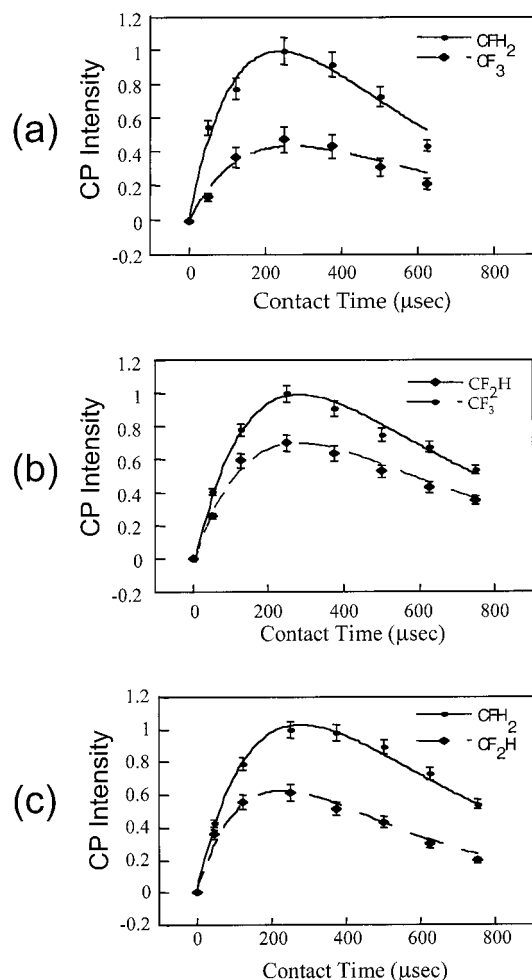


Figure 4. $^{19}\text{F} \rightarrow ^{23}\text{Na}$ CP intensity as a function of contact time ($\nu_{1\text{F}} = 20$ kHz; $\nu_{1\text{Na}} = 10$ kHz) (a) 4HFC-134a, (b) HFC-125 and (c) HFC-143/NaY_{2.6} at -120 °C. The curves were obtained with equations for CP intensity given in Eqs. [2–5].

polarization transfer rate, respectively, and β_I^0 is the initial inverse temperature of the I spins. To fit these curves, it was assumed, as a first approximation, that each end group is close to only one sodium cation (i.e., $N_S = 1$). $T_{1\rho}$ values for the ^{23}Na spins and the ^{19}F spins in the different end groups were all independently measured. The ^{19}F $T_{1\rho}$ s (170–320 μs) were found to be much shorter than those for ^{23}Na (~ 600 μs under the MAS and rf conditions used for CP) and are responsible for the relatively rapid decrease in CP intensity for contact times of greater than ~ 300 μs . The results obtained from fits to these curves with the measured $T_{1\rho}$ are shown in Table 3. The polarization transfer rates ($1/T_{1S}$) are larger for the more hydrogenated groups in the three systems. For example, values of T_{1S} of 480 ± 20 and 1000 ± 50 μs were obtained for the CFH₂ and CF₃ group, respectively, for HFC-134a/NaY_{2.6}. This indicates that the Na–F dipolar interaction involving the fluorine spins of the more hydrogenated groups is larger than that

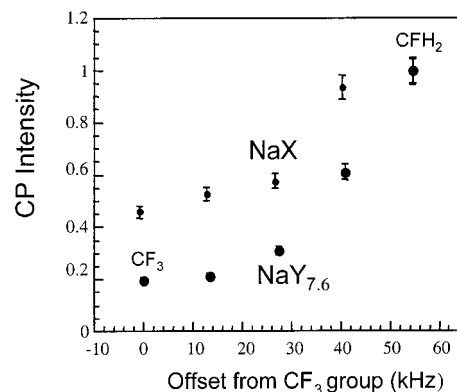


Figure 5. $^{19}\text{F} \rightarrow ^{23}\text{Na}$ CP intensity as a function of fluorine irradiation offset for NaX (small circles) and NaY_{7.6} (large circles) (Spinning speed = 8 kHz, $\nu_{1\text{F}} = 28$ kHz and $\nu_{1\text{Na}} = 14$ kHz (NaX); Spinning speed = 8 kHz; $\nu_{1\text{F}} = 20$ kHz; $\nu_{1\text{Na}} = 10$ kHz (NaY_{7.6})).

involving the fluorine spins of the other end groups. This may also indicate that the hydrogen-containing ends are, on average, coordinated to more sodium atoms.

Similar experiments have been performed with different zeolite samples (NaX and NaY_{7.6}) with different Si/Al ratios (i.e., different sodium contents), to explore the effect of the content of the sodium cations on the HFC binding. Two SI resonances at -4 and -11 ppm were observed in the ^{23}Na MAS spectrum of HFC-134a adsorbed on zeolite NaX, and are assigned to two different local environments following adsorption of HFC molecules, based on our earlier work for HFC-134 sorption on NaX.⁶ Broad resonances spreading from approximately -30 to -70 ppm are observed, which correspond to the site III' and II cations.⁶ The resonance from the site I' cations is not detected in the ^{23}Na MAS spectrum at a spinning speed of 10 kHz due to the large quadrupole coupling constant (> 5 MHz)²⁶ of this site and lies under the sidebands of the site II and III resonances. The two SI resonances are absent in the CP MAS spectra, whereas the broad SII/SIII resonances are observed. This implies that only the sodium cations in the supercage (the site III' and II cations) can interact with HFC molecules. Our previous ^{23}Na MAS and $^{19}\text{F} \rightarrow ^{23}\text{Na}$ CP MAS spectra obtained at a very fast spinning speed of 18 kHz have shown no evidence for cation migration and that the site I' cations do not interact with HFC molecules.⁵

Figure 5 compares the $^{19}\text{F} \rightarrow ^{23}\text{Na}$ CP intensity as a function of the offset frequency for 4HFC-134a/NaX and 4HFC-134a/NaY_{7.6}. The difference in the CP intensity for irradiation of the CFH₂ vs CF₃ groups in 4HFC-134a/NaX is very similar to that observed in the NaY_{2.6} system, but is much larger for 4HFC-134a/NaY_{7.6}. The smallest number of sodium cations are present in zeolite NaY_{7.6}, and this appears to result in the largest difference between the CP efficiency of the two end groups among the three zeolites (NaX, NaY_{2.6}, and NaY_{7.6}).

The $^{19}\text{F} \rightarrow ^{23}\text{Na}$ CP MAS experiments were also performed for HFC-134a on the three zeolites (NaX, NaY_{2.6}, and NaY_{7.6}), as a function of loading level, with the same ^{19}F rf field strength,

TABLE 3: Parameters Used in the Fits to the CP Curves, for On-resonance Irradiation of the CF₃, CF₂H, and CFH₂ Groups in HFC-134a, 125 and 143

	HFC-134a/NaY _{2.6}		HFC125/NaY _{2.6}		HFC143/NaY _{2.6}	
	CF ₃	CFH ₂	CF ₃	CF ₂ H	CF ₂ H	CFH ₂
scale ^a	0.22	0.18	0.12	0.12	0.18	0.18
$T_{1\rho,\text{F}}$ (μs)	205 ± 5	230 ± 5	205 ± 20	230 ± 20	170 ± 10	320 ± 10
T_{1S} (μs)	1000 ± 50	480 ± 20	1220 ± 100	845 ± 100	750 ± 50	560 ± 50

^a The parameter “scale” is a constant for each sample that is proportional to initial magnetization of the I spin (^{19}F), β_I^0 , as can be seen in eq 5.

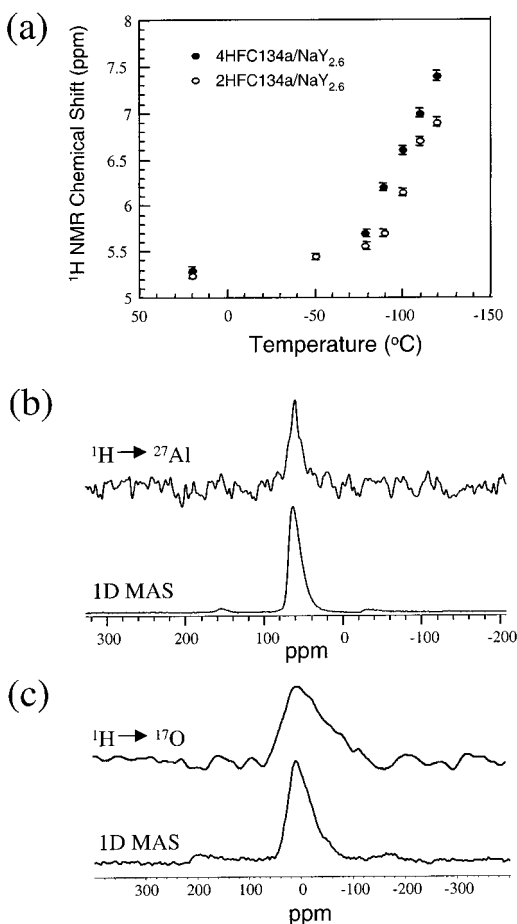


Figure 6. (a) ^1H chemical shift of 4HFC-134a/NaY_{2.6} as a function of temperature. (b) ^{27}Al MAS and $^1\text{H} \rightarrow ^{27}\text{Al}$ CP MAS spectrum of 4HFC-134a/NaY_{2.6} at -120°C (Spinning speed = 8 kHz; $\tau = 625 \mu\text{s}$; ν_{H} = 21 kHz; ν_{Al} = 7 kHz; number of acquisitions, $n_a = 9000$). (c) ^{17}O MAS and $^1\text{H} \rightarrow ^{17}\text{O}$ CP MAS spectrum of 4HFC-134a/NaY_{2.6} at -120°C (Spinning speed = 8 kHz; $\tau = 375 \mu\text{s}$; ν_{H} = 14 kHz; ν_{O} = 2 kHz; $n_a = 12000$).

TABLE 4: ^{23}Na CP Intensity for Experiments Performed with a ^{19}F offset Frequency Set On-resonance for the CF_3 Group, normalized to the Intensity of the Experiment with the ^{19}F Resonance Set On-Resonance for the CFH_2 Group, as a Function of Loading Level of HFC-134a

loading level	HFC-134a/NaY _{7.6}	HFC-134a/NaY _{2.6}	HFC-134a/NaX
1	0.23 (± 0.04)		
2		0.5 (± 0.05)	0.53 (± 0.05)
4	0.2 (± 0.04)	0.4 (± 0.05)	0.45 (± 0.05)
fully loaded			0.32 (± 0.03)

and the difference between the CP efficiencies from the two end groups was seen to increase as the loading level increased (Table 4). These results appear to indicate that the fraction of CF_3 groups bound to sodium cations decreases with increased loading level.

(b) ^1H VT, $^1\text{H} \rightarrow ^{27}\text{Al}$ and $^1\text{H} \rightarrow ^{17}\text{O}$ CP MAS. ^1H VT MAS, $^1\text{H} \rightarrow ^{27}\text{Al}$ and $^1\text{H} \rightarrow ^{17}\text{O}$ CP MAS experiments were performed, to probe the hydrogen bonding interaction between the hydrogen-containing groups and the zeolite framework. The ^1H chemical shift, measured as a function of temperature (Figure 6(a)), for 4HFC-134a adsorbed on NaY_{2.6} shifts to higher frequency by 2 ppm on lowering the temperature from room temperature to -120°C , consistent with an increase in the strength of H-bonding as the temperature is lowered. Both $^1\text{H} \rightarrow ^{27}\text{Al}$ and $^1\text{H} \rightarrow ^{17}\text{O}$ CP signals could be obtained at -120°C for 4HFC-134a/NaY_{2.6} (Figure 6b and (c), respectively), indicating the

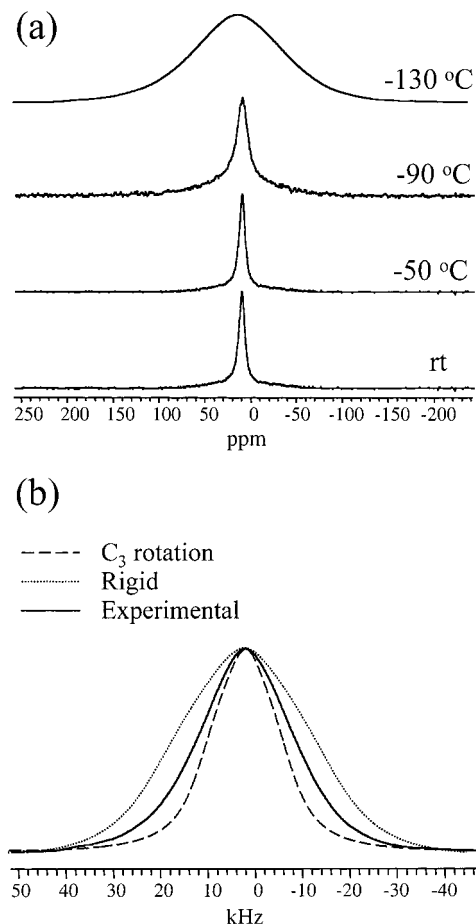


Figure 7. (a) ^1H static NMR spectra of 4HFC-134/NaY_{2.6} as a function of temperature. (b) Experimental ^1H static NMR spectra of 4HFC-134/NaY_{2.6} at -130°C and simulated spectra. H-F and F-F dipolar interactions of 14.8 and 10.4 kHz, respectively, were used for the simulation.

presence of short $^1\text{H}-^{27}\text{Al}$ and $^1\text{H}-^{17}\text{O}$ contacts. Previous high-resolution ^{17}O NMR experiments have shown that the quadrupole coupling constants (QCC) for the Si-O-Si oxygen local environments (~ 5.1 MHz) are larger than those of Al-O-Si oxygens (~ 3.5 MHz),²⁶ but that the resonances from these two local environments cannot be resolved in the ^{17}O MAS spectra at our field strength.²⁶ The resonance in the ^{17}O CP MAS spectrum is broader than that from the Al-O-Si and Si-O-Si oxygen atoms in bare NaY, indicating that the QCC of the framework oxygen atoms is increased due to the H-bonding interactions. H-bonding to the Si-O-Si oxygen atoms cannot be ruled on the basis of the ^{17}O (MAS) experiments alone, thus we have not analyzed these spectra any further to extract the QCCs. However, the observation of a ^{27}Al CP signal suggests that hydrogen bonding to Al-O-Si oxygen atoms must occur.

Variable temperature ^1H static NMR experiments were performed to investigate the dynamics of the end groups of the HFC molecules. The HFC-134 ($\text{CF}_2\text{HCF}_2\text{H}$) molecule was chosen for these studies since it has only one type of proton. Figure 7(a) shows the ^1H VT static NMR spectra of 4HFC-134 adsorbed on NaY_{2.6} at -130°C . The ^1H NMR resonance broadens significantly at temperatures lower than -100°C , primarily due to the increase in the H-F heteronuclear dipolar coupling. This line broadening occurs in the same temperature regime as the shift in the ^1H MAS NMR resonance to higher frequencies (Figure 6a). The static NMR line shape at -130°C was simulated by considering the heteronuclear dipolar

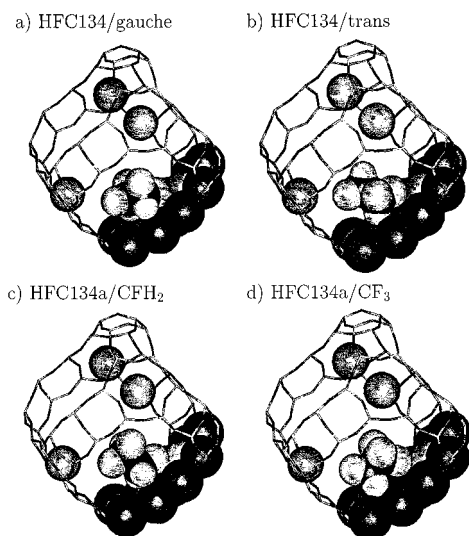


Figure 8. Minimum energy sites of HFC-134 and HFC-134a in faujasite model I (NaY, Si/Al = 2): absolute minimum energy sites for HFC-134 in (a) gauche and (b) trans conformations; absolute minimum energy sites for HFC-134a adsorbed on a Na(II) cation by (c) an F atom belonging to the CFH₂ group and (d) by the CF₃ group.

interactions (14.8 kHz) between the proton and two fluorine spins in the same end group (−CF₂H) only. The dipolar interactions between spins in different end groups were not included in the simulation. (These H–F and H–H dipolar interactions are 6.5 (6.8 and 3.3) and 4.2 (7.3) kHz, respectively, in *trans*-(*gauche*-) HFC-134). Figure 7b shows the experimental and simulated ¹H static NMR line shapes. The simulated NMR spectrum for a rigid end group is broader than the experimental spectrum, indicating that the motions of the end groups of HFC-134 are not completely frozen out, even at −130 °C. However, the experimental spectrum is slightly broader than the simulated spectrum performed assuming fast C₃ rotation of the end groups about the C–C bond, conditions under which the dipolar interaction is reduced by a factor of 2.²⁷

The ¹⁹F static NMR spectra of the HFC molecules adsorbed on NaX and NaY_{2.6} also contained a very broad resonance, on lowering the temperature to −130 °C, in this case broadened by both the chemical shift anisotropy and the dipolar interactions. The full width at half-maximum (fwhm) at −120 °C (~ 20 ± 4 kHz for the 4-HFC samples on both zeolites) was smaller than that at −130 °C (~ 40 ± 4 kHz, for both samples), indicating a freezing out of motion in this temperature regime, in the time scale of the ¹⁹F experiment. The HFC molecules are significantly more mobile in the lower sodium content zeolite, line widths (fwhm) of 7.4 and 5.4 kHz for the CFH₂ and CF₃ group, respectively, being observed even at −130 °C for 4HFC-134a/NaY_{7.6}.

These results suggest that although the end groups of the HFC molecules are not completely rigid at −120 °C, the temperature at which the CP experiments were performed, the isotropic motion appears to be significantly reduced.

Simulations. (a) *NaY (model I) Docking of HFC-134 and 134a.* The docking procedure located numerous energy minima, which were sorted into two classes for each molecule, with an energy dispersion for each class. In all cases, however, the HFC molecule is bound to a Na(II) cation by one F atom. Figure 8 shows examples of the minimum energy configuration for each class, whereas Table 5 summarizes some of the characteristics of each class. HFC-134 adsorbs either in a gauche configuration, with an F–C–C–F torsion angle (ϕ) near 60° (hereafter called HFC-134/*gauche*), or in a trans configuration, with $\phi \approx 180^\circ$

TABLE 5: Characteristics of the Minimum Energy Classes Resulting from the Docking of HFC-134 and HFC-134a in Model I

class	E_{\min} (kJ/mol)	ΔE (kJ/mol) ^a	dipole (D)	% structures ^b
HFC-134/ <i>gauche</i>	−70.1	26.9	3.8	68
HFC-134/ <i>trans</i>	−50.4	5.3	0.0	32
HFC-134a/FH ₂	−65.5	8.7	2.7	55
HFC-134a/F ₃	−57.3	13.8	2.7	45

^a Energy dispersion calculated as $\Delta E = E_{\max} - E_{\min}$. ^b % of the structures that fall in a given class during one docking calculation consisting of a hundred structures.

(hereafter called HFC 134/*trans*). HFC-134a binds to the cation either via an F atom belonging to the CF₃ group (HFC-134a/F₃), or to the CFH₂ group (HFC-134a/FH₂). HFC-134a/FH₂ configurations have significantly lower energies than do HFC-134a/F₃ configurations.

Table 5 shows that for HFC-134 in NaY, a rough correlation exists between the dipole and the minimum energy: the larger the dipole the lower the energy.³ For example, the large dipole in the *gauche* conformation (~3.8 D in our model) results in lower energies than for binding in the *trans* configuration, where the dipole is near zero. Although this simple correlation yields some insight into the binding interactions, the approach is clearly limited. In particular, the HFC-134a/FH₂ binding geometries are significantly lower in energy than the HFC-134a/F₃ geometries, due to the presence of hydrogen bonds in the former case. The distribution of binding energies clearly results from more detailed aspects of the HFC-zeolite interactions, than just those arising from the dipole moments.

The large dispersion of the minimum energies shows that there are several local minima, characterized by different NaF distances and O–H contacts. To shed some light on this behavior, we have analyzed the influence of two factors: (i) the Na–F distance, and (ii) the number and strength of O–H bonds. The latter is quantified with the following parameter

$$s_{\text{OH}} = \frac{\alpha_{\text{OH}}}{e^{-1}} \left(\sum_r \frac{e^{-r/\alpha_{\text{OH}}}}{r} \right) \quad (9)$$

where the sum extends over all O–H distances shorter than 9 Å. α_{OH} is set to 2.6 Å, hence, the parameter s_{OH} provides a measure of the number of O–H bonds with an average length of 2.6 Å for the whole HFC molecule (i.e., both end groups). In principle, both the NaF distance and s_{OH} correlate with more favorable host–guest interactions: shorter NaF distances and larger s_{OH} values should result in lower energies. Figure 9 presents a plot of E vs s_{OH} and d_{NaF} for all minimum energy configurations resulting from docking of HFC-134 and HFC-134a in model I. For HFC-134 in NaY, considered separately in the *gauche* and *trans* configurations, we observe a correlation between the energy and both s_{OH} and d_{NaF} : E decreases as either s_{OH} increases or d_{NaF} decreases, as expected. A similar correlation is observed between the energy and s_{OH} for HFC-134a, in both the FH₂ and F₃ configurations. On the other hand, we note a negative correlation between the energy and d_{NaF} , which is contrary to what was expected. This would appear to suggest that the main factor influencing the energy of HFC-134a in NaY is the number and strength of O–H bonds, whereas the NaF distance is only of secondary importance. Note, however, that Na–FH₂ configurations, which generally have lower energies than Na–F₃ configurations, have shorter NaF distances, whereas s_{OH} is generally the same for both binding arrangements. This suggests that Na–FH₂ configurations are stabilized over Na–

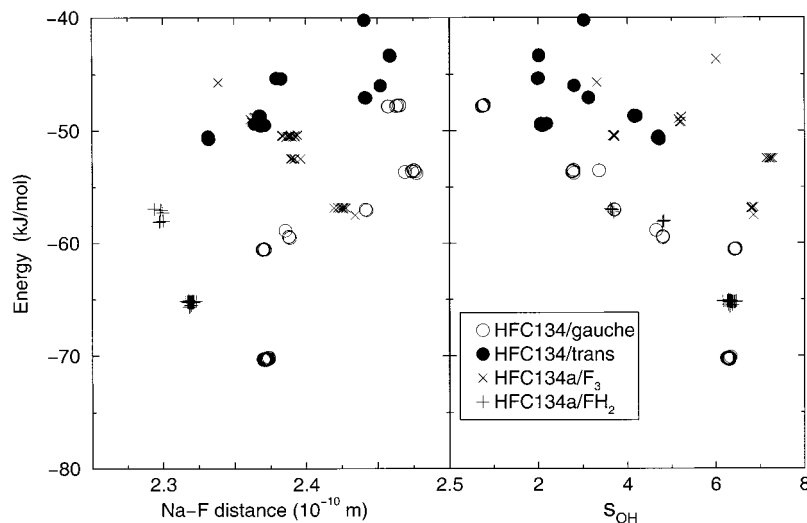


Figure 9. Minimum energy of HFC-134 and HFC-134a in faujasite model I (NaY, Si/Al = 2), as a function of the Na(II)-F distance (left) and the parameter s_{OH} defined in the text (right).

F_3 configurations, by the possibility of achieving shorter NaF distances, for the same number of O-H hydrogen bonds.

(b) *NaY (model I) Molecular Dynamics of HFC-134 and 134a.* Molecular dynamics simulations were performed in NaY starting from the minimum energy positions in both Na-FH₂ and Na-F₃ configurations for HFC-134a, and in gauche and trans conformations for HFC-134. We found that the HFC-134a molecule, in a 300 K MD run starting from an Na-F₃ binding mode, quickly jumps through the supercage and relaxes to form an FH₂-Na(II) contact; this behavior was also observed at 200 K. Therefore, for these temperatures the Na-F₃ docking site appears to be unstable. On the other hand, the high torsional energy barrier between trans and gauche conformations of HFC-134 prevents any interchange between the sites during the time of an MD run at these temperatures.

A graphical analysis of the trajectory reveals that HFC-134a bound via an F atom of the CFH₂ group on a Na(II) cation remains linked to this cation during the entire MD duration; two independent 0.4 ns runs were performed to check this behavior. At 300 K, the HFC-134a molecule can rotate almost freely around the C₃ axis of NaY running through the Na(II) cation on which it is bound and the center of the supercage. Indeed, a plot of the O-Na-F-C torsion angle distribution (not shown) does not reveal any significant structure. HFC-134 in both gauche and trans conformations also exhibits some rotation around the same C₃ axis. In addition, however, we observe frequent jumps between Na(II) cations inside the supercage, with the Na-F contact changing from one F₂H group to the other. Although several of these jumps are observed during the time of the simulation (about 10), the number remains too small to deduce a statistically meaningful time constant for this motion.

The O-H and NaF pair distribution functions (PDF), calculated from the MD runs at 300 K for HFC-134a, HFC-134/gauche, and HFC-134/trans are shown in Figure 10. All NaF PDFs exhibit sharp peaks at 2.3 Å, corresponding to the principal NaF contact. The peak is sharper for HFC-134a, indicating a more rigid binding site. The other peaks at 4.5 and 5.8 Å correspond to the other Na(II) cations in the same supercage, for which there is no direct Na-F contact. The O-H PDFs show much more variability among the molecules. In particular, HFC-134 in a trans configuration has less favorable O-H contacts than both HFC-134/gauche and HFC-134a. The HFC-134a O-H PDF has a much sharper structure than for

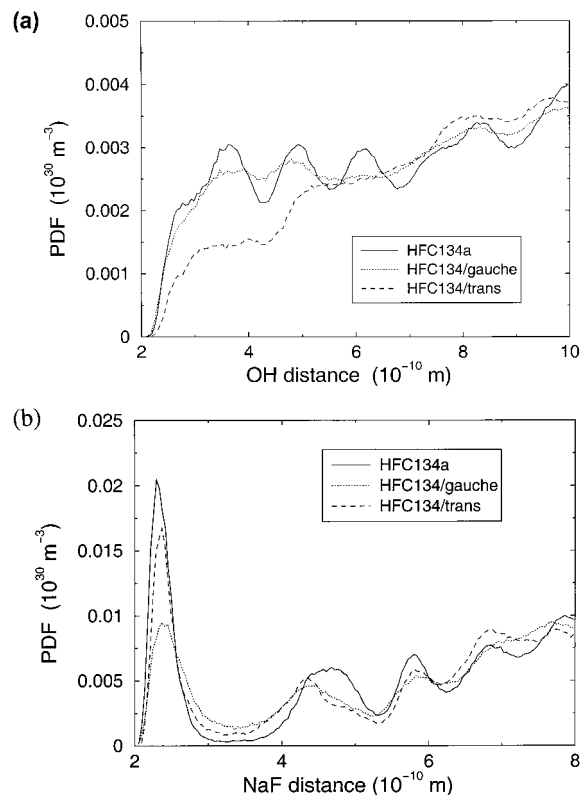


Figure 10. (a) O-H and (b) NaF pair distribution functions for HFC-134 and HFC-134a adsorbed in faujasite model I (Si/Al = 2), as calculated from a 0.4 ns MD run at 300 K.

HFC-134, with well-defined peaks indicating either lower vibrational amplitude or lower translational mobility of this molecule.

(c) *NaX (model II) Docking of HFC-134 and 134a.* The different types of energy minima located by the docking procedure for these HFCs in NaX are very similar for HFC-134a and HFC-134, in both gauche and trans configurations, but they appear rather different from what was found in NaY (model I). In NaX, we find many different energy minima where the adsorbate is coordinated by either zero, one, two or three fluorine atoms to one or more Na cations. Table 6 summarizes the characteristics of the different sites. For example, the '3

TABLE 6: Characteristics of the Minimum Energy Classes Resulting from the Docking of HFC-134 and HFC-134a in NaX (model II)

class	E_{\min} (kJ/mol)	ΔE (kJ/mol) ^a	% structures ^b
HFC-134/gauche/0 NaF	-101.6	8.3	12
HFC-134/gauche/1 NaF	-95.2	17.3	23
HFC-134/gauche/2 NaF	-100.3	40.3	32
HFC-134/gauche/3 NaF	-98.9	31.1	9
HFC-134/trans/1 NaF	-74.2	21.2	7
HFC-134/trans/2 NaF	-84.8	31.0	8
HFC-134/trans/3 NaF	-94.3	9.6	10
HFC-134a/0 NaF	-79.9	13.4	9
HFC-134a/1 NaF	-85.6	17.5	46
HFC-134a/2 NaF	-86.5	38.3	28
HFC-134a/3 NaF	-95.4	33.9	17

^a Energy dispersion calculated as $\Delta E = E_{\max} - E_{\min}$. ^b Percentage of the structures that fall in a given class during one docking calculation involving a hundred structures.

NaF' site involves an HFC molecule linked to 1 Na(II) and 1 Na(III) cation at one end, and to another Na(III) cation at the other end.

As in NaY, we find that the minimum energies correlate with the dipole: the lowest energy was observed for HFC-134 in a gauche conformation (-101.6 kJ/mol), while higher energies are observed for HFC-134a (-95.4 kJ/mol) and for HFC-134 in a trans conformation (-94.3 kJ/mol). However, these facts have little to do with the interactions between fixed molecular dipoles and supercage Na cations. In particular, the most stable HFC-134/gauche binding geometry involves zero close Na-F contacts. In addition, the energies of different HFC-134/gauche local minima do not correlate with the number of Na-F contacts, indicating that a more subtle balance between Na-F and O-H contacts is at play.

To explore this issue, we have studied the influence of close O-H and Na-F contacts on the adsorption energy, as for model I. Close O-H contacts are defined by the same s_{OH} parameter introduced in the preceding section. Since we observe more than one close Na-F contact for HFCs in NaX, such contacts are now quantified by the following parameter, in analogy with s_{OH}

$$s_{NaF} = \frac{\alpha_{NaF}}{e^{-1}} \sum_r \frac{e^{-(r/\alpha_{NaF})^2}}{r} \quad (10)$$

with $\alpha_{NaF} = 2.3 \text{ \AA}$. Plots of energy vs s_{OH} and s_{NaF} (not shown) do not appear to exhibit any correlation with s_{NaF} for HFC-134/gauche, and only a slight negative correlation with s_{NaF} for HFC-134/trans. On the other hand, there is a clear correlation between the energy and the s_{OH} for HFC-134/gauche, whereas s_{OH} is limited to a maximum value around 4 for HFC-134/trans. This limit is due to the trans configuration, which prevents the favorable O-H contacts between the framework oxygen and the two H atoms of HFC-134 at the same time. HFC-134a does not show any clear trend with s_{OH} or s_{NaF} : the minimum energy sites are those with three Na contacts, but sites with multiple H-bonding interactions are reasonably close in energy. As with model I, these results show that O-H contacts do appear to be an important factor influencing the energy.

Savitz et al.³ reported a heat of adsorption at low loading and 26.2 °C of 75.1 kJ/mol for HFC-134 in NaX, and 64.9 kJ/mol for HFC-134a in NaX at low loading and 25.7 °C. The minimum interaction energies determined for these molecules in model II are clearly much larger in absolute terms: indeed, using the approximation $q^{st} = -U_{\min} - k_B T$, we find $q^{st} \approx 105$ kJ/mol for HFC-134 and $q^{st} \approx 98$ kJ/mol for HFC-134a.

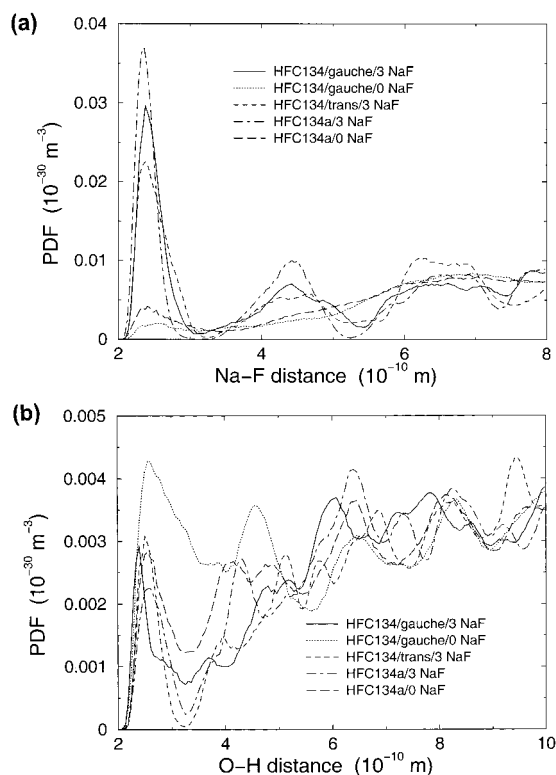


Figure 11. (a) Na-F and (b) O-H pair distribution functions for HFC-134 and HFC-134a adsorbed in faujasite model II (Si/Al = 1), as calculated from 0.4 ns MD run at 200 K.

Considering the energy averaged over the 100 docked structures, however, leads to heats of adsorption that are closer to the experiment: 86.8 kJ/mol for HFC-134, and 79.5 kJ/mol for HFC-134a. The difference between the adsorption energies of HFC-134a and HFC-134 follows the experimental trend, and is of the same order of magnitude. This agreement is acceptable when we consider that the force field used in this study was not specifically parametrized for guest adsorption in zeolites, in contrast to most force fields used in this field.

(d) *NaX (model II) Molecular Dynamics of HFC-134 and 134a.* Several MD calculations were initiated from each class of minimum energy sites found by the docking procedure, to investigate the motions of the molecules. We have identified two distinct behaviors, depending on whether the run was started from a '0 Na-F' site or a '3 Na-F' site. The '1 Na-F' and '2 Na-F' cases were either indistinguishable from the '3 Na-F' or '0 Na-F' runs, or exhibited intermediate behavior. Figure 11 shows the Na-F and O-H PDFs for the MD runs initiated from the 5 sites presented in Table 6 (i.e., HFC-134/gauche in a '3 Na-F' and a '0 Na-F' site, HFC-134/trans in a '3 Na-F' site, and HFC-134a in a '3 Na-F' and a '0 Na-F' site). The Na-F PDF is qualitatively very similar for the three runs started from a '3 Na-F' site and is also similar for the two runs initiated at a '0 Na-F' site. This shows that in NaX, *the type of adsorption site has more influence on the adsorbate's motions than the arrangement of the H/F atoms in the particular HFC isomer.* The O-H PDFs, on the other hand, are markedly different for the two runs initiated in '0 Na-F' sites, namely HFC-134/gauche and HFC-134a. The docking calculation predicted roughly the same number of O-H bonds for HFC-134/gauche and HFC-134a in '0 Na-F' sites. MD, therefore, reveals that close O-H contacts stabilize HFC-134/gauche more than HFC-134a, which is consistent with the stability of HFC-134/gauche/0 Na-F sites shown in Table 6. The peaks of the

O–H PDF are much narrower in NaX (model II) than in NaY (model I), showing that these molecules are much more constrained at their positions in NaX. Indeed, we do not observe any translational or rotational motion such as was observed in NaY.

4. Discussion

Overview of Experimental Findings. $^{19}\text{F} \rightarrow ^{23}\text{Na}$ CP NMR experiments demonstrate that the efficiency of the CP process is very sensitive to the ^{19}F -irradiation offset; this has been exploited to investigate CP from different HFC end groups. In HFC-125, the frequency separation of the resonances from the two end groups is smaller than the ^{19}F rf field strength, indicating that CP transfer from one end group (e.g., CFH_2) may contribute to the $^{19}\text{F} \rightarrow ^{23}\text{Na}$ CP signal, even when the irradiation frequency is on-resonance for the other end group (e.g., CF_2H) (see eq 1). It is, however, clear that for *all* molecules, maximum CP efficiency is always achieved for irradiation at the frequency of the end group containing the largest numbers of hydrogen atoms; results from attempts to deconvolute the plots of CP efficiency vs offset, by using eq 1 are consistent with this statement. These observations suggest that the more-hydrogenated groups are bound more effectively to the zeolite framework, resulting in the higher CP intensity. The differences in CP intensities between the different end groups become larger with increasing gas loading level, and as the temperature is decreased.

Diffraction and NMR studies for $\text{NaY}_{2.6,5,28}$ have shown that, even for loading levels as low as 2 HFC-134 molecules per supercage, sodium migration occurs, so that at low temperatures ($-120\text{ }^\circ\text{C}$) and moderate loading levels, the HFC molecules are bound to at least 2 sodium atoms per HFC, and the concentration of sodium cations in the supercages is similar to that in NaX. This is consistent with the very similar differences between the CP efficiency of the two end groups of HFC-134a adsorbed on $\text{NaY}_{2.6}$ and NaX: similar numbers of sodium cations will be present in the supercages of both systems for the binding of the HFC molecules because no changes in the occupancy of the site I' cations are observed on adsorption of HFC molecules onto zeolite NaX.⁶

The shift in the ^1H resonance with temperature, and the $^1\text{H} \rightarrow ^{17}\text{O}$ and $^1\text{H} \rightarrow ^{27}\text{Al}$ CP NMR results both suggest that hydrogen bonding of the HFC molecule to the zeolite framework occurs.

Overview of Simulation Findings. The docking calculations reveal preferential adsorption of HFC-134 over HFC-134a in models of faujasite with both low and high Al content, i.e., NaY and NaX, respectively. For all molecules in NaY (model I), the minimum energy configurations involve a single Na–F contact at an average distance of $\sim 2.4\text{ \AA}$. The binding of HFC-134a in NaY is more favorable with a $\text{CFH}_2\text{--Na(II)}$ geometry than it is with $\text{CF}_3\text{--Na(II)}$, by ca. 8 kJ/mol. This simulation result is qualitatively consistent with the CP results. MD results reveal that at 200 and 300 K, only the 'FH₂' site is a stable adsorption site in NaY. The docking results suggest that this is due to the possibility of achieving a slightly shorter Na(II)–F distance in the FH₂ case, while maintaining the same number of O–H bonds.

In NaX (model II), HFC-134a and HFC-134 in a gauche configuration can exhibit favorable contacts with either 0, 1, 2, or 3 Na cations. Fewer Na–F contacts are compensated by more favorable O–H contacts: the '0 Na–F' site actually constitutes the global energy minimum for HFC-134/gauche. Because of its geometry, HFC-134 in a trans conformation cannot form as

many O–H bonds as its gauche conformer, or as HFC-134a. As a consequence, no '0 Na–F' binding modes are found for HFC-134/trans. The analysis of the minimum energies found by docking reveals that the main factor influencing the energy, apart from the ion–dipole interaction, is the number of O–H contacts. MD simulations show that both '3 Na–F' sites and '0 Na–F' sites remain stable adsorption sites for 0.4 ns at 300 K, and that the molecules in these sites do not show any significant translational or rotational motion, such as was observed in NaY.

The faujasite models have Si/Al ratios of 2 and 1 for models I and II, respectively. The locations of cations in these simulations were held fixed, a typical approximation in simulations of dry zeolites. This prevents any cation migration during the simulations, in contrast to the experiments that show some migration from sites I' in the sodalite cages to sites III in the supercages, upon adsorption of HFC-134.⁵ However, because the cation migration observed experimentally only arises with HFC loadings of at least 8 molecules per unit cell, whereas our simulations were run with only 1 molecule per unit cell, keeping the cations fixed in our present simulations is a good first approximation. In a forthcoming publication, we will report simulations of HFC adsorption in NaX and NaY where cations are allowed to move simultaneously alongside HFC molecules.

Comparison of Experimental and Simulation Results. Differences in the experimental CP intensity are due, in principle, to two causes: differences in (i) Na–F dipolar coupling, and (ii) spin-locking of the F/Na nuclei. Fits to the contact time plots (Figure 4) rule out the second possibility and demonstrate that the differences in CP intensities are due to variations in T_{1S} (see Table 3) and, hence, from differences in the dipolar couplings between the end groups and the extraframework cations. Again, there are, in principle, three possible causes: differences in (i) Na–F distances, (ii) the number of coupled spins, or (iii) the averaging of the Na–F dipolar coupling due to the effects of residual motion. If the CP efficiency were controlled by the numbers of coupled fluorine spins, an increase in CP intensity from CFH_2 to CF_3 is predicted, contrary to experimental findings. The docking calculations presented above reveal small variations in Na–F distances for $\text{CF}_2\text{H--Na}$ and $\text{CF}_3\text{--Na}$ for HFC-134/NaY (model I), but these differences are not large enough to explain fully the large differences seen in T_{1S} in Table 3. The calculations clearly demonstrate that, for low sodium concentrations, where the HFC molecule may only bind to one Na cation (model I), the HFC-134a molecule preferentially binds to Na(II) with the CFH_2 end group. This is consistent with the CP results, particularly for the low sodium content zeolite $\text{NaY}_{7.0}$. Furthermore, the increase in difference between the CP efficiency of the end groups as a function of loading level is consistent with a competition between the two end groups for the available Na cations and for the optimum binding sites.

The CP MAS NMR experiments were performed at temperatures where the motion of the HFC molecules is only just starting to freeze out in the time scale of the ^1H and ^{19}F NMR experiments: The ^{19}F static NMR spectra of the HFC molecules in 4-HFCs/ $\text{NaY}_{2.6}$ are relatively sharp at $-120\text{ }^\circ\text{C}$ (fwhm $\sim 20\text{ kHz}$), in comparison to that at $-130\text{ }^\circ\text{C}$ (fwhm $\sim 40\text{ kHz}$), while the experimental ^1H static NMR spectrum at $-130\text{ }^\circ\text{C}$ was only slightly broader than the simulated spectrum for the fast C_3 rotation of the end group. This is consistent with earlier studies of CF_3 groups, which in solid silver trifluoroacetate ($\text{CF}_3\text{--COOAg}$) are known to undergo a fast C_3 rotation even at $-166\text{ }^\circ\text{C}$.²⁹ This implies that C_3 rotation of the end groups may also

be present at the temperature of $-120\text{ }^{\circ}\text{C}$, where the CP MAS experiments were performed. The MD simulations, however, suggest that alternative dynamics may be more important, particularly for the low-sodium content material: calculations for NaY ($\text{Si}/\text{Al} = 2.0$) show that hops involving motion of the HFC-134a about the C_3 axis through the Na(II) cation and the center of the supercage, *maintaining a Na-F(HFC) contact throughout*, are also important, while for HFC molecules containing H atoms on both ends (i.e., HFC-134), hops from one SII to the adjacent SII can occur. Since these motions are observed in the MD simulation time scale (ca. 100 ps), they are likely to occur in the so-called fast regime in the NMR experiment, where motions of the order of 0.1–10 ms are probed. Rotation of the HFC-134a molecule about the C_3 axis will lead to a reduction of the ^1H – ^1H dipolar coupling by approximately a factor of 0.5, consistent with the static ^1H spectrum of this molecule at low temperature. These motions are not, however, isotropic and, thus, although they will reduce the Na–F dipolar couplings for both CF_3 and CFH_2 end groups, a larger residual Na–F coupling involving the directly bound CF_2H group is clearly expected for HFC-134a. The plot of the PDF for HFC-134a in model I (Figure 10) reveals a sharp peak at 2.3 Å, which is sharper than that of HFC-134 trans and gauche, consistent with a stable Na– FCH_2 binding arrangement and the presence of a residual Na–F dipolar coupling.

As the Na content increases, the calculations show that the HFC molecules are more tightly bound to the more negative framework and cations, due to the larger number of Na–F interactions and stronger O–H interactions (due to the higher charge on the oxygen atoms). This is consistent with the NMR results, where an increase in the ^{19}F line widths at $-130\text{ }^{\circ}\text{C}$ from $\text{fwhm} = 7.4$ and 5.4 kHz for the CFH_2 and CF_3 groups, respectively, in 4HFC-134a/NaY_{7.6}, to 40 kHz for 4HFC-134a in NaX and NaY, was observed, consistent with decreased motion in the higher Al-content zeolite. Furthermore, this decrease in motion for the higher Al-content systems is associated with a smaller difference between the CP intensities for the two end groups in HFC-134a.

On the basis of the results from both NMR and calculations, the differences in CP efficiency from the two groups appears to be due to two major causes. The preferential binding of the CFH_2 groups to the Na cations, results in (i) reduced Na– CF_3 dipolar couplings, since not all the CF_3 groups are bound to cations, and (ii) more effective averaging of the Na– CF_3 dipolar coupling, in the temperature regime where the CP experiments were performed.

Both the NMR and calculations indicate that H-bonding plays a very important role in defining the binding arrangements. The pronounced shift in the ^1H resonance of HFC-134a to higher frequency, as the temperature is lowered, indicates that the binding energies that represent energy minima and which presumably become increasingly populated at lower temperatures, are those involving strong H-bonding to the framework. The correlation between the number of hydrogen bonds, so_H , obtained by simulation and the binding energy is consistent with this picture. The importance of hydrogen bonding in these types of systems is consistent with earlier work (calculations and inelastic neutron scattering studies) for hydrofluorocarbons and hydrochlorocarbons.^{8,9}

The binding modes suggested by our NMR and docking results should be contrasted with the structure of HFC-134 bound to NaY found from low-temperature X-ray diffraction.⁵ Here, the HFC-134 molecules were found to bind to an average of between one and two sodium atoms. In these experiments,

we were unable to distinguish between the trans and gauche conformers. Raman studies for HFC-134 in NaX showed that the gauche isomer becomes increasingly stabilized relative to the trans isomer on sorption on NaX, consistent with the much lower binding energies found for this conformer.⁸ It is clear, however, that the stability of the gauche form is not only due to the dipole moment of this conformer, but due to the possibility of forming multiple H-bonding contacts with the framework.

5. Conclusions

By applying solid state NMR and molecular simulations, we have found that the binding of even such relatively simple molecules as the HFCs may not be fully understood by considering simple electrostatic arguments involving molecular dipoles. This is clearly illustrated for HFC-134a binding where, based on the dipole of this molecule, CF_3 –Na interactions are predicted to be favored over CFH_2 –Na interactions. The reverse is found above both experimentally and by calculations. Careful analysis of the results from theory and experiment suggests that the actual binding arrangement of the molecule is controlled by local electrostatic interactions involving a combination of H-bonding with the framework, and with the sodium cations. Docking calculations for HFC-134a suggest that the stronger binding of the CF_2H group, in comparison to the CF_3 group, to the Na cations is due to the possibility of achieving a slightly shorter Na(II)–F distance in the FH_2 case, while maintaining the same number of O–H bonds. As the charge of the framework increases and the strength of the H-bonding interactions increase, binding arrangements involving H-bonding only, and no short Na–F contacts may actually represent global energy minima.

The theoretical results have been used to help corroborate many of the experimental findings. For example, modes of motion were identified in by the MD simulations, involving both translation and rotations. These would have been difficult to predict from the NMR results since the NMR methods used here are sensitive to rotations only. The simulations suggested that it is the difference in the averaging of the Na–F dipolar coupling (which is controlled by both motion- and preferential binding to Na of the hydrogen containing groups) that controls the differential CP efficiencies for each end group of the molecule.

The CP experiments show that is possible to investigate differential interactions between different parts of a molecule with the surface *without* resorting to chemical labeling of selective atoms, but by exploiting the sensitivity of the CP efficiency to the offset frequency. Although the large chemical shift range of ^{19}F clearly made these experiments feasible, the increasingly routine use of higher field instruments should allow these types of experiments to be become more widely applicable to other nuclei (such as ^{31}P and ^{13}C). The demonstrated feasibility of ^1H – ^{17}O CP experiments for this system suggests many new applications of CP involving molecules and the oxygen atoms of the framework, to probe basicity and in some cases determine which oxygen sites are involved in binding. Furthermore, our recent results show that by combining the CP experiment with a multiple pulse or Lee-Goldberg sequence (in a HETCOR experiment), it may be possible to determine which hydrogen atoms are involved in the H-bonding.

Finally, these results help explain the trends in separation factors of Y zeolites² for the HFC-134/134a separations and heats of adsorption ($\text{HY} < \text{LiY} < \text{NaY} < \text{CsY}$); CsY has the most basic framework in the series of monovalent cation-exchanged zeolites Y, and thus the strongest hydrogen bonding results.

Acknowledgment. C.P.G. thanks the Department of Energy, Basic Energy Sciences Division for support via DEFG0296ER14681. S.M.A. gratefully acknowledges support from the National Science Foundation (Career CTS-9734153), a Sloan Foundation Research Fellowship (BR-3844), and a Camille Dreyfus Teacher-Scholar Award (TC-99-041).

References and Notes

- (1) Manzer, L. E. *Science* **1990**, *249*, 31. Manzer, L. E.; Webb, G.; Winfield, J. *Chemistry in Britain* **1992**, *28*, 996. Rao, V. N. M. *Adv. Catal.* **1993**, *39*, 329.
- (2) Corbin, D. R.; Mahler, B. A. World Patent, W. O. 94/02440 (February 3, 1994).
- (3) Savitz, S.; Siperstein, F. R.; Huber, R.; Tieri, S. M.; Gorte, R. J.; Myers, A. L.; Grey, C. P.; Corbin, D. R. *J. Phys. Chem. B* **1999**, *103*, 8283.
- (4) Grey, C. P.; Corbin, D. R. *J. Phys. Chem.* **1995**, *99*, 16821.
- (5) Grey, C. P.; Poshni, F. I.; Gualtieri, A. F.; Norby, P.; Hanson, J. C.; Corbin, D. R. *J. Am. Chem. Soc.* **1997**, *119*, 1981.
- (6) Lim, K. H.; Grey, C. P. *J. Am. Chem. Soc.* **2000**, *122*, 9768.
- (7) Lim, K. H.; Grey, C. P. *Chem. Commun.* **1998**, *20*, 2257.
- (8) Udovic, T. J.; Nicol, J. M.; Cavanagh, R. R.; Rush, J. J.; Crawford, M. K.; Grey, C. P.; Corbin, D. R. *Mater. Res. Soc. Symp. Proc.* **1995**, *376*, 751. Crawford, M. K.; Dobbs, K. D.; Smalley, R. J.; Corbin, D. R.; Maliszewskij, N.; Udovic, T. J.; Cavanagh, R. R.; Rush, J. J.; Grey, C. P. *J. Phys. Chem. B* **1999**, *103*, 431.
- (9) Mellot, C. F.; Cheetham, A. K.; Harms, S.; Savitz, S.; Gorte, R. J.; Myers, A. L. *J. Am. Chem. Soc.* **1998**, *120*, 5788. Mellot, C. F.; Cheetham, A. K.; Harms, S.; Savitz, S.; Gorte, R. J.; Myers, A. L. *Langmuir* **1998**, *14*, 6728. Mellot, C. F.; Cheetham, A. K. *J. Phys. Chem. B*, **1999**, *103*, 3864.
- (10) Bielecki, A.; Burum, D. P. *J. Magn. Reson. A* **1995**, *116*, 215.
- (11) Vega, A. J. *J. Magn. Reson.* **1992**, *96*, 50.
- (12) Vega, A. J. *Solid State Nucl. Magn. Reson.* **1992**, *1*, 17.
- (13) Ferguson, D. B.; Krawietz, T. R.; Haw, J. F. *J. C. S.; Chem. Commun.* **1995**, 1795.
- (14) De Paul, S. M.; Ernst, M.; Shore, J. S.; Stebbins, J. F.; Pines, A. *J. Phys. Chem. B* **1997**, *101*, 3240.
- (15) Smith, S. A.; Levante, T. O.; Meier, B. H.; Ernst, R. R. *J. Magn. Reson. A* **1994**, *106*, 75.
- (16) Cheng, V. B.; Suzukawa, H. H.; Wolfsberg, M. *J. Chem. Phys.* **1973**, *59*, 3992.
- (17) Auerbach, S. M.; Henson, N. J.; Cheetham, A. K.; Metiu, H. I. *J. Phys. Chem.* **1995**, *99*, 10600. Auerbach, S. M.; Bull, L. M.; Henson, N. J.; Metiu, H. I.; Cheetham, A. K. *J. Phys. Chem.* **1996**, *100*, 5923.
- (18) Fitch, A. N.; Jobic, H.; Renouprez, A. *J. Phys. Chem.* **1986**, *90*, 1311.
- (19) Vitale, G.; Mellot, C. F.; Bull, L. M.; Cheetham, A. K. *J. Phys. Chem. B* **1997**, *101*, 4559.
- (20) Jousse, F.; Auerbach, S. M. unpublished 1998.
- (21) Mellot, C. F.; Davidson, A. M.; Eckert, J.; Cheetham, A. K. *J. Phys. Chem. B* **1998**, *102*, 2530.
- (22) George, A. R.; Freeman, C. M.; Catlow, C. R. A. *Zeolites* **1996**, *17*, 466.
- (23) Henson, N. J.; Auerbach, S. M. DIZZY Computational Chemistry Program 1994–1998.
- (24) Mehring, M. *Principles of High-Resolution NMR in Solids*, 2nd ed.; Springer-Verlag: New York 1983.
- (25) Walter, T. H.; Turner, G. L.; Oldfield, E. *J. Magn. Reson.* **1998**, *76*, 106.
- (26) Timken, H. K. C.; Janes, N.; Turner, G. L.; Lambert, S. L.; Welsh, L. B.; Oldfield, E. *J. Am. Chem. Soc.* **1986**, *108*, 7236. Bull, L. M.; Cheetham, A. K.; Anupold, T.; Reinhold, A.; Samoson, A.; Sauer, J.; Bussemer, B.; Lee, Y.; Gann, S.; Shore, J.; Pines, A.; Dupree, R. *J. Am. Chem. Soc.* **1998**, *120*, 3510. Pingel, U.-T.; Amoureux, J.-P.; Anupold, T.; Bauer, F.; Ernst, H.; Fernandez, C.; Freude, D.; Samoson, A. *Chem. Phys. Lett.* **1998**, *294*, 345.
- (27) Slichter, C. P. *Principles of Magnetic Resonance*, 3rd ed.; Springer-Verlag: New York 1989.
- (28) Ciruolo, M. F.; Hanson, J. C.; Grey, C. P. *J. Phys. Chem. B*, submitted.
- (29) Mehring, M.; Griffin, R. G.; Waugh, J. S. *J. Chem. Phys.* **1971**, *55*, 746.